Published in final edited form as:
ACS Appl Mater Interfaces. 2009 December ; 1(12): 2747–2754. doi:10.1021/am9005435.

Centrifugal Deposition of Microgels for the Rapid Assembly of Nonfouling Thin Films

Antoinette B. South[†,‡], **Rachel E. Whitmire**[‡,§,⊥], **Andrés J. García**[‡,⊥], and **L. Andrew Lyon**[*,†,‡]

School of Chemistry and Biochemistry, Petit Institute for Bioengineering and Bioscience, Wallace H. Coulter Department of Biomedical Engineering, and Woodruff School of Mechanical Engineering, Georgia Institute of Technology, Atlanta, Georgia 30332

Abstract

Thin films assembled from microgel building blocks have been constructed using a simple, high-throughput, and reproducible centrifugation (or “active”) deposition technique. When compared to a common passive adsorption method (e.g., dip coating), microgels that are actively deposited onto a surface have smaller footprints and are more closely packed. Under both active and passive deposition conditions, the microgel footprint areas decrease during deposition. However, under active deposition, the microgel footprint appears to decrease continually and to a greater degree over the course of the deposition, forming a tightly packed, homogeneous film. Taking advantage of the rapid and uniform assembly of these films, we demonstrate the use of active deposition toward the fabrication of polyelectrolyte multilayers containing anionic microgels and a cationic linear polymer. Microgel multilayers successfully demonstrated effective blocking of the underlying substrate toward macrophage adhesion, which is a highly sought-after property for modulating the inflammatory response to an implanted biomaterial.

Keywords

hydrogel particles; centrifugation; film interfaces; layer by layer; cellular adhesion

INTRODUCTION

The construction of polymeric thin films is a subject of significant industrial importance for drug delivery (1), wettability control (2), corrosion (3), or cellular adhesion inhibition (4), as well as of fundamental interest. Over the past few decades, a number of fabrication techniques have been employed to form films from a variety of building blocks, and their versatility has been demonstrated. Whereas extensive research has been conducted in the use of linear polymers (5–8) and continuous hydrogel networks (9–12) as polymeric interfaces, recent investigations into the use of solvent-swollen polymer colloids, or microgels, have illustrated the utility of colloidal gels as building blocks (13–18). When the solvent is water,

[*]To whom correspondence should be addressed. lyon@chemistry.gatech.edu.
[†]School of Chemistry and Biochemistry.
[‡]Petit Institute of Bioengineering and Bioscience.
[§]Wallace H. Coulter Department of Biomedical Engineering.
[⊥]Woodruff School of Mechanical Engineering.

Supporting Information Available: AFM images and corresponding line profiles of microgel films at selected time points of deposition, under both passive and active deposition for both microgel types, a figure illustrating the size of the AFM tip relative to the microgels, and AFM images comparing active and passive deposition techniques under low and high ionic strength buffers. This material is available free of charge via the Internet at http://pubs.acs.org.

microgels are composed of a water-soluble polymer cross-linked into a contiguous network, with the diameters of the particles typically ranging from ~100 nm to many micrometers (19–21). When stimulus-sensitive polymers are used (such as pH-sensitive (22) or thermoresponsive (23) polymers) to form microgels, those particles and the resulting films can then exhibit responsive behavior by undergoing a volume phase transition as a function of that stimulus (13). Given their growing importance in film formation, microgels have been used as building blocks in the construction of films with potential utility in drug release (24,25), tunable microlenses (26,27), colloidal crystals (28–30), and nonfouling films (31–33). These interfaces have been assembled using a variety of deposition techniques such as dip coating (34–40), spin coating (24,25,31–33,41,42), or solvent evaporation (16,29,30). In addition, different hierarchical structures havebeenaccomplishedbylayer-by-layerassembly(24,25,34,41), binary particle mixtures (39), or phase-separation-induced deposition (16).

One particularly important aspect of film formation is control over the deposited material. For biomedical coatings, for example, the hydrophobicity, morphology, elasticity, and chemistry of a synthetic material's surface can have a dramatic effect on the cell phenotype and behavior (43). Furthermore, complete coverage of the underlying substrate is typically desired in order to ensure total control of cell adhesion, spreading, and proliferation. Hydrogel-based materials can be fabricated to possess characteristics that make them suitable as a biomaterial because their volume consists mostly of water when in an aqueous environment and they are highly tunable in terms of their mechanical properties and chemical composition. Additionally, in a particulate form, microgels enable further complexity by enabling the assembly of multifunctional interfaces, because of a mixture of various types of microgels that can simultaneously assemble on the same surface, along with additional interesting morphologies. It is this ability to easily tune and adjust an interface that makes microgels an appealing material for controlling and studying how proteins, cells, and tissues interact with a synthetic interface.

In this contribution, we report a film fabrication approach that employs centrifugation to assemble microgel films in a fast, efficient, and reproducible manner. Whereas centrifugation has been used beyond the traditional use of purification, such as in the preparation of liposomes (44), rapid patterning of cells (45), or high-speed fabrication of photonic microfluidics (46), to our knowledge, little has been explored in using centrifugation as a polymer film deposition technique. In this work, we have demonstrated for the first time the use of centrifugation to fabricate microgel-based films and explore what effect this additional parameter or force may have on the assembly of microgel monolayers. Our initial hypothesis was that centrifugation would simply decrease the amount of time it would take to create a continuous and uniform monolayer, as compared to a passive process. However, upon further investigation, it was evident that using centrifugation (referred to herein as "active" deposition) to force the hydrated particles onto a hard substrate resulted in an assembly that had smaller and more closely packed particles than what could be ultimately obtained with simple microgel adsorption ("passive" deposition). To evaluate the generality of this phenomenon, a model system consisting of two microgel particles of different sizes was studied. In addition, possible mechanisms for the observed results were briefly explored. Last, we illustrate the technique's ability to construct rapid multilayered polyelectrolyte layer-by-layer films for the fabrication of effective uniformnonfouling coatings to prevent macrophageadhesion.

MATERIALS AND METHODS

Materials

All reagents were purchased from Sigma-Aldrich unless otherwise specified. The monomer *N*-isopropylacrylamide (NIPAm) was recrystallized from hexanes (J. T. Baker) and dried under vacuum prior to use. The cross-linkers *N*,*N*′-methylenebis(acrylamide) (BIS) and poly(ethylene glycol) diacrylate (PEG-DA) with average M_w = 575 (PEGDA575), comonomer acrylic acid (AAc), and initiator ammonium persulfate (APS) were used as received. Buffer chemicals sodium dihydrogen phosphate monohydrate (Fisher Scientific), 2-(*N*-morpholino)-ethanesulfonic acid (MES), sodium chloride (Mallinckrodt), and sodium hydroxide were used as received. The surface modification reagent (3-aminopropyl)trimethoxysilane (APTMS; TCI America) was used as received. Covalent attachment chemicals *N*-hydroxysuccinimide (NHS), *N*-[3-(dimethylamino)propyl]-*N*′-ethylcarbodiimide hydrochloride (EDC), and hydroxylamine hydrochloride were used as received. High-molecular-weight (400 000–500 000) poly(diallyldimethylammonium chloride) (PDADMAC) was used as received. Glass disks of 12-mm diameter were purchased from Bellco Glass. Absolute (200 proof) ethanol was used as received from EMD Chemicals Inc. All water used throughout this investigation was house-distilled, deionized to a resistance of at least 18 MΩ (Barnstead Thermolyne E-Pure system). The IC-21 murine macrophage cell line was obtained from ATCC (Manassasa, VA) and cultured as directed. RPMI-1640 media were purchased from Gibco (Invitrogen Corp., Carlsbad, CA) and/or ATCC (Manassas, VA), supplemented with 10% fetal bovine serum (FBS; Invitrogen) and 1% penicillin streptomycin (PS; Gibco) and used to culture the IC-21 cell line. Tissue culture polystyrene (TCPS) dishes (100 and 150 mm; Corning Inc., Corning, NY) were used to culture cells. Phosphate-buffered saline (PBS, with and without calcium and magnesium) was obtained from Gibco. Versene (Gibco) was used to dissociate the cells from the dishes. Plates (12-well) from Corning Inc. (Corning, NY) were bought via Sigma-Aldrich (St. Louis, MO) and used for the cell culture experiments. Calcein and ethidium homodimer were bought from Invitrogen Corp. (Carlsbad, CA) and used at final concentrations of 4 μM to stain for live and dead cells.

Microgel Synthesis

Microgels were synthesized using aqueous free-radical precipitation polymerization. Microgel **1** was synthesized using a total monomer concentration of 70 mM with a molar composition of 85% NIPAm, 5% BIS, and 10% AAc. Surfactant sodium dodecyl sulfate (SDS) was used at a concentration of 1 mM. All of these components were dissolved in 49 mL of deionized water and filtered through Whatman No. 2 filter paper in a vacuum filtration system. The aqueous solution was then transferred to a three-neck, round-bottomed flask and purged with N_2 for approximately 1 h while the solution was heated to 70 °C. The initiator APS (0.0114 g), used in a total final concentration of 1 mM, was dissolved in 1 mL of deionized water and added to initiate polymerization. The reaction was allowed to proceed for 4 h at 70 °C under a blanket of N_2.

Microgel **2** was synthesized using a total monomer concentration of 100 mM, with a molar composition of 88% NIPAm, 2% BIS, and 10% AAc. Surfactant SDS and initiator APS were used in concentrations of 0.17 and 1 mM, respectively. The remaining conditions of the synthesis were carried out in the same fashion as that described for **1**.

Nonfouling microgels were synthesized using a total monomer concentration of 100 mM with a molar composition of 88% NIPAm, 2% PEGDA575, and 10% AAc. Surfactant SDS and initiator APS were used in concentrations of 0.17 and 1 mM, respectively. The

remaining conditions of the synthesis were carried out in the same fashion as that described for **1**.

Microgel Characterization

Dynamic light scattering (DLS) was used as previously described (28,47) to measure the hydrodynamic radius and diffusion coefficient of synthesized particles. A Protein Solutions DynaPro equipped with a temperature-controlled microsampler was used for these measurements. Light scattering data were collected at intervals of 10 s per reading with a photodiode detector fixed at 90° relative to the incident laser light (783.9 nm). Dynamics Software was used to calculate the autocorrelation decay from the random fluctuations in the scattered light intensity. This information was then used to determine the diffusion coefficient of the sample in solution, which correlates with the hydrodynamic radii of the particles using the Stokes–Einstein equation. Electrophoretic mobility measurements were performed with a Malvern Instruments Zetasizer. All measurements were conducted using a dilute solution of microgels in a pH 7.4 phosphate buffer containing 100 mM ionic strength (PBS).

Film Preparation

The 12-mm-diameter glass coverslip disks were placed in a ceramic glass slide holder and cleaned using a sequential solvent sonication method. A sequential solvent sonication method proceeded with the following solvent sequence using a Bransonic 2510 ultrasonicator (42 kHz ± 6% output): 30 min in dilute soapy (Alconox) water, 15 min in deionized water, 15 min in acetone, 15 min in absolute ethanol, and 15 min in isopropyl alcohol. Afterward, the glass was immediately equilibrated for 30 min in absolute ethanol, and 1% by volume APTMS was added. The glass was incubated with the APTMS/ethanol solution for 2 h under gentle agitation. The disks were then rinsed with a 70% aqueous ethanol solution and deionized water and then dried under a gentle stream of N_2.

Cleaned and dried glass disks were individually placed at the bottom of 24-well plates, and PBS was immediately added. The glass was allowed to equilibrate for 30 min, and the buffer was then replaced with a 0.1 mg/mL solution of microgels in a pH 7.4 phosphate buffer containing 100 mM ionic strength (PBS). For centrifuged films, the well plates were placed immediately opposite to a counterweighted well plate in an Eppendorf 5804R centrifuge equipped with a plate-holding rotor. Films were centrifugally deposited at a maximum rotor speed of 2250*g* for a specific amount of time. Passively adsorbed microgel films were made by control of the exposure time of the functionalized glass to the microgel solution. After deposition, the films were rinsed with deionized water and dried under a gentle stream of N_2. All films were deposited at room temperature.

Samples prepared using nonfouling microgels were deposited using a 0.8 mg/mL microgel solution in PBS. Centrifugation was carried out at 2250*g* for 5 min at room temperature. Afterward, the monolayers were covalently attached to the amine-functionalized glass by activation of the acids on the particles. To accomplish this, EDC/NHS bioconjugation chemistry was employed. A solution containing 2 mM EDC and 5 mM NHS was prepared in a 10 mM MES buffer (pH 6) and allowed to react with the nonfouling microgel film for 2 h at room temperature. After the films were rinsed with water, they were exposed to a 10 mM solution of hydroxylamine in a MES buffer for 10 min to quench the EDC/NHS reaction. The films were then rinsed with water to remove excess reagents.

Multilayer Formation

In the past, our group has amply demonstrated the use of microgels in the fabrication of multilayered thin films (24,25,34,41). In this study, microgel monolayer films were

constructed using active deposition in the same fashion as that described above. To add an additional layer, a 0.14 monoM (molar concentration of monomer) solution of PDADMAC was added to the film and allowed to adsorb to the microgel film for 30 min. The films were then washed five times with deionized water. Another layer of microgels was then added to the well and centrifuged onto the surface, as described above. This process was repeated until four microgel layers were deposited. The thickness of the microgel multilayer film was determined by using a razor blade to scratch the surface of the film and expose the underlying substrate, and atomic force microscopy (AFM) was used to determine the height of the film relative to the substrate.

AFM Imaging and Analysis

Microgel films were imaged using an Asylum Research MFP-3D Instrument (Santa Barbara, CA). Imaging was performed and processed using the MFP-3D software under the IgorPro (WaveMetrics Inc., Lake Oswego, OR) environment. Noncontact-mode, aluminum-coated silicon nitride cantilevers were purchased from NanoWorld (force constant = 42 N/m; resonance frequency = 320 kHz). All images were taken in noncontact mode, in air under ambient conditions. For all images, a set-point ratio (set-point amplitude/free oscillation amplitude) of ~0.75 was used to ensure reproducible mechanical interactions between the tip and sample.

Quantitative image analysis was performed to calculate the average particle footprint area on the glass surface. Briefly, an iterative inverse mask was created to highlight the particles, and the image was flattened to the second order. A histogram was then generated to evaluate the bimodal distribution of the surface height and particle height. Three times the standard deviation of the surface height was added to the average height of the surface to account for variations in the surface around the particles. A new inverted mask was generated based on this calculation, and the percentage of the image that was masked was calculated. This percentage was divided by the number of particles (counted manually) to give an average particle footprint area. The radial distribution function for the images was calculated using code written in-house in the IDL version 6.1 programming environment.

In Vitro Cellular Adhesion Studies

Microgel multilayer films were sterilized after assembly in a 70% ethanol aqueous solution. Before use with cells, films were washed three times in sterile PBS and then equilibrated in fresh PBS for at least 1 h before use. A murine peritoneal macrophage cell line, IC-21, was employed to test for adhesion to the multilayer films in vitro. Macrophages are one of the primary mediators of the inflammatory response and can fuse to form the foreign-body giant cells that make up a significant portion of the fibrous capsule around an implanted biomaterial. The use of a macrophage cell line is standard for examining the nonfouling behavior in vitro due to this cell type's extremely adhesive nature and the role in the body's response to a biomaterial. The IC-21 cell line is a virally transformed murine peritoneal macrophage line that expresses many of the standard macrophage surface proteins and maintains the phagocytic and cytolytic behaviors characteristic of untransformed macrophages. IC-21 cells were cultured in RPMI-1640 media supplemented with 10% FBS and 1% PS. The cultures were grown at 37 °C with 5% CO_2. The cells were removed using Versene, counted by a hemacytometer, and then diluted to a concentration of 200 000 cells/1.5 mL of media. The microgel films were placed in a sterile 12-well culture dish, and 1.5 mL of cells/media was added. The films were incubated at 37 °C for 4 h, after which the excess media/cells were aspirated and samples were transferred to new wells and fresh media. Samples were incubated overnight and stained the next day with 4 μM calcein and ethidium homodimer in PBS. Samples were imaged at 20× magnification with a Nikon Eclipse E400 upright microscope (Nikon Instruments, Inc., Melville, NY). Images were

taken with Spot Advanced software (Diagnostic Instruments, Sterling Heights, MI). Eight representative images were taken per sample, with three samples per group. Cells were counted using the public domain NIH ImageJ program (developed at the U.S. National Institutes of Health and available on the Internet at http://rsb.info.nih.gov/nih-image/). The cell count was averaged over all representative images of the same sample type, and the error bars shown represent the standard error for the group of three samples.

RESULTS AND DISCUSSION

To study assembled microgel monolayers using the active centrifugation deposition technique, two different anionic microgel particles composed of NIPAm, AAc, and the cross-linker BIS were synthesized; these particles were used in the coulombically driven assembly of microgel films onto cationic silane-modified glass substrates. The particles were characterized using DLS and AFM; the results of these characterizations are summarized in Table 1. The hydrodynamic radius of particle **1** is roughly half that of particle **2** because of differences in the cross-linker density, total monomer concentration in the reaction, and amount of surfactant used in the synthesis. Accordingly, the diffusion coefficient for **1** is twice as large as that of **2**. Additionally, **2** has an approximately 6 times larger footprint area when passively adsorbed onto a surface and is slightly softer than **1**, as evidenced by the higher R_s/R_h (radius on the surface/radius in solution) ratio. However, both particle types have similar electrophoretic mobilities. Therefore, any differences seen under centrifugal deposition will be due to differences in the sedimentation velocity, not the surface accessibility of anionic charges on the particle for attachment to the cationic substrate.

Centrifugal, or active, deposition is performed by placing the substrates of interest at the bottom of each well in a multiwell plate (e.g., a cell culture plate), followed by the addition of a microgel dispersion into the well above the substrate. The plates are then placed in a swinging bucket, well-plate rotor. When the rotor spins, the well plates swing out so as to align the centrifugal force (*g*), perpendicular to the plane of each substrate, thereby forcing the colloidal particles onto the substrate. For all experiments described in this study, the maximum centrifugal force of the rotor (2250*g*) was used. Because of its utility in the deposition of films on multiple samples simultaneously, centrifugal film deposition is fast and reproducible and many samples can be made in parallel with a high degree of quality control.

Microgels **1** and **2** were both subject to active film deposition, with passive deposition being used as a comparison throughout this entire study. AFM was used previously to study passively adsorbed microgel particle monolayers (40), and those studies clearly illustrated the utility of the technique in this domain. It is important to point out that the microgels were dispersed and deposited in a PBS solution of high ionic strength (100 mM); these conditions have previously been shown to be appropriate for reducing anionic repulsion between microgels during film formation (39). Our initial observations illustrate that microgels that are actively deposited form films that are fundamentally different from those deposited passively. As can be seen in Figure 1, when active deposition is used (Figure 1b,d), the microgels appear to be smaller and more closely packed than those deposited passively (Figure 1a,c). This difference in the particle size is perhaps more clearly seen when smaller scan sizes are used (Figure 1 insets). It is also worth noting that, regardless of the deposition method, the particles all have heights of only ~10–15 nm in the dehydrated state, illustrating the extremely low polymer density of the particles, as we have described previously (39,41). The calculated radial distribution functions for these images, also shown in Figure 1, quantitatively illustrate the differences in the particle spacing and nearest-neighbor probability. Both microgels **1** and **2** show nearest-neighbor distances that are closer under

active deposition, thus confirming that these films are more tightly packed when actively deposited as compared to passive adsorption. Interestingly, one might expect that microgels would flatten under centrifugal force and therefore result in particles with larger footprint areas and a film with a decreased particle density. However, the opposite is apparent in these experiments, which likely indicates that the particles have some lateral mobility on the surface. The exact origin of this phenomenon is unclear, but it is likely that the presence of salt in the medium acts to screen the coulombic interactions between the surface and the microgels, which would decrease the microgel–surface affinity.

The evolution of the microgel films was monitored as a function of the deposition time under both active and passive conditions (Figure 2). The larger microgels **2** appeared to reach full coverage faster than the smaller microgels **1** when centrifuged onto a surface. This is expected because of larger or more massive particles having a higher sedimentation velocity. The opposite was true for the passively adsorbed microgels because the smaller particles have a higher diffusion coefficient and therefore reach the surface faster, which should result in faster coverage assuming an equivalent sticking probability. In addition, the particle footprint area was monitored as a function of time. Under both deposition conditions and for both microgel types, the microgel footprints appeared to decrease during deposition. However, under active deposition, the microgels appeared to shrink to smaller footprints than those obtained via passive deposition, and they also appeared to shrink over a range of deposition times. We consider the possibility that tip convolution could be an issue when imaging particles that are spaced closely together, which would result in microgels that would appear to be smaller in the *x*, *y*, and *z* dimensions. However, our data suggest that the AFM tip is effectively reaching the underlying substrate because no loss in the microgel height is observed as the particle spacing is decreased (see the Supporting Information). We also provide a scale illustration of the particle dimensions with respect to the AFM tip, which also suggests that tip convolution should not introduce significant error in our analyses because the particle heights are so small relative to the tip dimensions. There are a few possible mechanisms by which active deposition might result in smaller microgels that pack more tightly. For example, centrifugation could cause the microgels to concentrate in the solution above the substrate and thus deswell because of an increase in the local osmotic pressure (48–50). Alternatively, the use of a high ionic strength buffer (100 mM) during deposition could permit the particles to desorb or rearrange on the surface, thereby dynamically reconfiguring the interface as microgels continue to strike the interface at a high velocity. Finally, it may be the case that actively deposited microgels have somewhat different adsorption/adhesion characteristics than those of passively deposited microgels. It is worth noting that while the particle sizes decrease during deposition, the final footprints do not approach the fully collapsed or dehydrated state of the microgels, which would be 2–4-fold smaller than that observed here. Thus, the particle footprints are more representative of the swollen particles, with some size decrease due to an additional factor such as those suggested above.

Considering these possibilities, it is unlikely that microgel preconcentration during centrifugation is exclusively responsible for these observations because small particle footprints might be expected early in the deposition as well. However, Figure 2 clearly shows that the microgels are initially larger and grow smaller over time during film assembly. Therefore, a dynamic rearrangement at the interface must be occurring during the formation of the film, under both active and passive deposition conditions, with the effect persisting even after the formation of a high-coverage monolayer under active conditions. To further explore this phenomenon, we used a two-step deposition method, the results of which are shown in Figure 3. In this experiment, microgels were first adsorbed passively to obtain partial coverage (Figure 3a) or to obtain a higher coverage (Figure 3b), and then without replacement of the microgels or removal of the film from solution, the samples were

subjected to active (centrifugal) microgel deposition conditions. The results illustrate that, under these conditions, the average particle footprint area does still decrease upon active deposition but not to the same extent as that observed during active deposition alone. Additionally, if particles are first passively adsorbed until a high-coverage monolayer is generated, additional centrifugation does not induce a statistically meaningful change in the adsorbed microgel size. These data suggest that the passively adsorbed microgels do not rearrange dramatically or desorb from the surface during further active deposition. When space is available for microgels to deposit (Figure 3a), it appears that lateral repulsion between microgels might result in some decrease in microgel footprint and particle rearrangement. However, when microgels centrifuged on top of the passively deposited particles are unable to make their way onto the substrate (Figure 3b), significant restructuring of the interface is not observed. These results are in agreement with a previous study using similar pNIPAm-*co*-AAc microgels adsorbed on an amine-modified surface, where the authors illustrated that even with increasing NaCl concentrations there was no evidence of particle desorption from the surface (35). Considering these results, it is therefore likely that particle adsorption is fundamentally different between the two cases. Passive adsorption likely results in a polymer chain conformation that is closer to the thermodynamic minimum, whereas the active approach results in a polymer conformation that is higher in energy (kinetically determined) and is therefore more likely to evolve and age during centrifugation. This theory is further reiterated by observing the impact of the ionic strength of the dispersion buffer on film assembly. When microgels are dispersed in a lower ionic strength buffer (2 mM), there is also a noticeable difference in the microgel size and spacing (see the Supporting Information). Though the particles are not as small and highly packed as under high ionic strength (100 mM) conditions, because of reduced shielding of repulsive side chains, active deposition once again results in a smaller size and spacing of microgels on the surface compared to passive deposition. This observation suggests that, even when shielding of the anionic side chains is significantly reduced, centrifugation can still overcome particle–particle repulsion to a greater extent than a dip-coating method, presumably because of the higher energy used in deposition.

The recent work of FitzGerald et al. (40) seems to support the hypothesis that particles can reorganize laterally because of interparticle repulsion. These investigators studied the passive adsorption of pH-sensitive microgel particles using liquid AFM imaging. Their results demonstrate the dynamic nature of such particles at the particle–surface interface. When these particles are in their nondeformable latex form at higher pH, they observe a significant deviation from what is expected from the random sequential adsorption model of hard spheres, where the diameter of the particles at the interface is almost twice the size of that in solution. Furthermore, when the pH was adjusted to more acidic conditions, thus inducing a latex-to-swollen microgel transition, this swelling pressure caused neighboring particles to desorb from the surface. Even though coulombic interactions exist between the particle and substrate, the particle–particle interactions dominate in their example. These results illustrate an extreme case of dynamic microgel adsorption where lateral particle interactions can dictate particle coverage. Similarly, our results illustrate that polymeric particles can undergo size changes and film rearrangement as a function of coverage, albeit in the limit of strong microgel–surface interactions.

Multilayered polyelectrolyte microgel interfaces, which we demonstrated previously (24,25,34,41), were fabricated using rapid centrifugal film deposition to illustrate the utility of the technique. The progression of layers of a multilayered microgel film is shown in Figure 4. Atop a glass substrate that was rendered cationic by amine functionalization, anionic microgels (microgel **2**) were alternatively layered with PDADMAC as a cationic polymer. As more layers are added (up to four layers of microgels), less of the underlying glass substrate appears to be exposed, and the resulting film is quite uniform. The average

film height for the four-layer film is ~60 nm in the dry state, as determined by AFM line profiles across a scratch in the film introduced by a clean razor blade. In light of these results, we constructed multilayers of nonfouling microgels to aid in the prevention of cellular adhesion to a surface. In the past, we have used spin coating to fabricate a monolayer of nonfouling microgels containing the cross-linker PEG-DA (31–33). PEG is a polymer widely known to resist protein and cellular adhesion because of its high degree of hydration and conformational flexibility (4,51–53). Previously, we showed that spin coating of nonfouling microgels onto a substrate provided the high coverage needed to block the background substrate from protein and cellular adhesion. However, spin coating is an intrinsically serial process that can be quite wasteful of material. However, as discussed below, centrifugation-based assembly can be parallelized and also provides the required high coverages using a rapid multilayering approach in a nonwasteful manner.

The results in Figure 5 demonstrate the effectiveness of actively deposited nonfouling microgel multilayers toward the blocking of macrophage adhesion. Macrophages adhere and spread well on the positive-control TCPS. Glass that was extensively cleaned also shows cellular adhesion and spreading, with an approximately 5-fold reduction in the number of cells adhering compared to TCPS. However, four-layer microgel films, which were generated quickly using centrifugation deposition, showed significant blockage of macrophage adhesion, with an over 200-fold and over 30-fold reduction in the number of adherent cells compared to TCPS and cleaned glass, respectively. Furthermore, the few cells that adhere to the surface of the microgel multilayer films do not appear to be able to spread, and therefore it is speculated that these cells have found small defects in the film, which presumably could be blocked with additional layers. Optimization of the film properties in the context of nonfouling biomaterial coatings will be the subject of later studies.

CONCLUSIONS

Centrifugation has been demonstrated to be a rapid and robust method for generating colloidal films. When using hydrated anionic microgel particles to construct an interface, centrifugation deposition results in particles that are smaller and more closely packed compared to a more common dip coating, or passive adsorption technique. The footprint area of centrifuged particles actively shrinks during the course of assembly. Passively deposited microgels appear to stop decreasing in the footprint size at an earlier stage in the adsorption process, and when these films are subsequently subjected to centrifugally forced microgel deposition, the centrifugation approach does not force significant morphological changes in the deposited particles. The impact of this phenomenon on the particle adhesion, modulus, and film stability is currently being explored in our laboratories. In addition, it has been demonstrated that the centrifugal deposition approach enables a functional multilayered microgel interface with a high degree of uniformity and substrate coverage. These interfaces can be used in the development of microstructured hydrogel coatings for control of biological and cellular adhesions and exploited for various other applications in which complexity, tunability, and uniformity are desired.

Supplementary Material

Refer to Web version on PubMed Central for supplementary material.

Acknowledgments

We thank the Nils Kröger group for the use of their Zetasizer instrument. We also thank Prof. K. C. Chan (Albany State University, Physics) for discussions about radial distribution functions and Jae Kyu Cho (Georgia Institute of Technology, ChBE) for help using the IDL program for calculating radial distribution functions. Furthermore, we thank the Georgia Institute of Technology for providing GTEC II funding for this research.

REFERENCES AND NOTES

1. Yoshida M, Langer R, Lendlein A, Lahann J. Polym Rev 2006;46(4):347–375.
2. Motornov M, Sheparovych R, Tokarev I, Roiter Y, Minko S. Langmuir 2007;23(1):13–19. [PubMed: 17190478]
3. Cho SH, White SR, Braun PV. Adv Mater 2009;21(6):645.
4. Lopez GP, Ratner BD, Tidwell CD, Haycox CL, Rapoza RJ, Horbett TA. J Biomed Mater Res 1992;26(4):415–439. [PubMed: 1601898]
5. De Gennes PG. Adv Colloid Interface Sci 1987;27(3–4):189–209.
6. Douglas JF, Johnson HE, Granick S. Science 1993;262(5142):2010–2012. [PubMed: 17794964]
7. van de Ven TGM. Adv Colloid Interface Sci 1994;48:121–140.
8. Kaellrot N, Linse P. Macromolecules 2007;40(13):4669–4679.
9. Kim SW, Bae YH, Okano T. Pharm Res 1992;9(3):283–290. [PubMed: 1614957]
10. Kirker KR, Luo Y, Nielson JH, Shelby J, Prestwich GD. Biomaterials 2002;23(17):3661–3671. [PubMed: 12109692]
11. Schmaljohann D, Oswald J, Jorgensen B, Nitschke M, Beyerlein D, Werner C. Biomacromolecules 2003;4(6):1733–1739. [PubMed: 14606903]
12. Shu XZ, Liu Y, Palumbo F, Prestwich GD. Biomaterials 2003;24(21):3825–3834. [PubMed: 12818555]
13. Nayak S, Lyon LA. Angew Chem, Int Ed 2005;44(47):7686–7708.
14. Lyon LA, Meng Z, Singh N, Sorrell CD, John AS. Chem Soc Rev 2009;38(4):865–874. [PubMed: 19421566]
15. Hendrickson GR, Lyon LA. Soft Matter 2009;5(1):29–35.
16. Lynch I, Miller I, Gallagher WM, Dawson KA. J Phys Chem B 2006;110(30):14581–14589. [PubMed: 16869558]
17. Wei YY, Luo YW, Li BF, Li BG. Colloid Polym Sci 2006;284(10):1171–1178.
18. Ugur S, Elaissari A, Yargi O, Pekcan O. Colloid Polym Sci 2007;285(4):423–430.
19. Pelton R. Adv Colloid Interface Sci 2000;85(1):1–33. [PubMed: 10696447]
20. Jones CD, Lyon LA. Macromolecules 2000;33(22):8301–8306.
21. Gan DJ, Lyon LA. J Am Chem Soc 2001;123(31):7511–7517. [PubMed: 11480971]
22. Saunders BR, Crowther HM, Vincent B. Macromolecules 1997;30(3):482–487.
23. Wu X, Pelton RH, Hamielec AE, Woods DR, McPhee W. Colloid Polym Sci 1994;272(4):467–477.
24. Nolan CM, Serpe MJ, Lyon LA. Biomacromolecules 2004;5(5):1940–1946. [PubMed: 15360309]
25. Serpe MJ, Yarmey KA, Nolan CM, Lyon LA. Biomacromolecules 2005;6(1):408–413. [PubMed: 15638546]
26. Kim J, Serpe Michael J, Lyon LA. J Am Chem Soc 2004;126(31):9512–9513. [PubMed: 15291534]
27. Serpe MJ, Kim J, Lyon LA. Adv Mater 2004;16(2):184–187.
28. Debord JD, Lyon LA. J Phys Chem B 2000;104(27):6327–6331.
29. Hellweg T, Dewhurst CD, Eimer W, Kratz K. Langmuir 2004;20(11):4330–4335. [PubMed: 15969135]
30. McGrath JG, Bock RD, Cathcart JM, Lyon LA. Chem Mater 2007;19(7):1584–1591.
31. Nolan CM, Reyes CD, Debord JD, Garcia AJ, Lyon LA. Biomacromolecules 2005;6(4):2032–2039. [PubMed: 16004442]
32. Singh N, Bridges AW, Garcia AJ, Lyon LA. Biomacromolecules 2007;8(10):3271–3275. [PubMed: 17877399]
33. Bridges AW, Singh N, Burns KL, Babensee JE, Lyon LA, Garcia AJ. Biomaterials 2008;29(35):4605–4615. [PubMed: 18804859]
34. Serpe MJ, Jones CD, Lyon LA. Langmuir 2003;19(21):8759–8764.

35. Nerapusri V, Keddie JL, Vincent B, Bushnak IA. Langmuir 2006;22(11):5036–5041. [PubMed: 16700591]
36. Nerapusri V, Keddie JL, Vincent B, Bushnak IA. Langmuir 2007;23(19):9572–9577. [PubMed: 17685638]
37. Hoefl S, Zitzler L, Hellweg T, Herminghaus S, Mugele F. Polymer 2007;48(1):245–254.
38. Schmidt S, Hellweg T, von Klitzing R. Langmuir 2008;24(21):12595–12602. [PubMed: 18847289]
39. Sorrell CD, Lyon LA. Langmuir 2008;24(14):7216–7222. [PubMed: 18553989]
40. FitzGerald PA, Dupin D, Armes SP, Wanless EJ. Soft Matter 2007;3(5):580–586.
41. Sorrell CD, Lyon LA. J Phys Chem B 2007;111(16):4060–4066. [PubMed: 17407344]
42. Schmidt S, Motschmann H, Hellweg T, von Klitzing R. Polymer 2008;49(3):749–756.
43. Anderson JM. Annu Rev Mater Res 2001;31:81–110.
44. Zhang L, Hu J, Lu Z. J Colloid Interface Sci 1997;190(1):76–80. [PubMed: 9241144]
45. Barrett DG, Yousaf MN. Angew Chem, Int Ed 2007;46(39):7437–7439.
46. Lee SK, Yi GR, Yang SM. Lab Chip 2006;6(9):1171–1177. [PubMed: 16929396]
47. Yi YD, Bae YC. J Appl Polym Sci 1998;67(12):2087–2092.
48. St John AN, Breedveld V, Lyon LA. J Phys Chem B 2007;111(27):7796–7801. [PubMed: 17579396]
49. St John AN, Lyon LA. J Phys Chem B 2008;112(36):11258–11263. [PubMed: 18710277]
50. Meng Z, Cho JK, Breedveld V, Lyon LA. J Phys Chem B 2009;113(14):4590–4599. [PubMed: 19298093]
51. Gombotz WR, Wang GH, Horbett TA, Hoffman AS. J Biomed Mater Res 1991;25(12):1547–1562. [PubMed: 1839026]
52. Jeon SI, Andrade JD. J Colloid Interface Sci 1991;142(1):159–166.
53. Pale-Grosdemange C, Simon ES, Prime KL, Whitesides GM. J Am Chem Soc 1991;113(1):12–20.

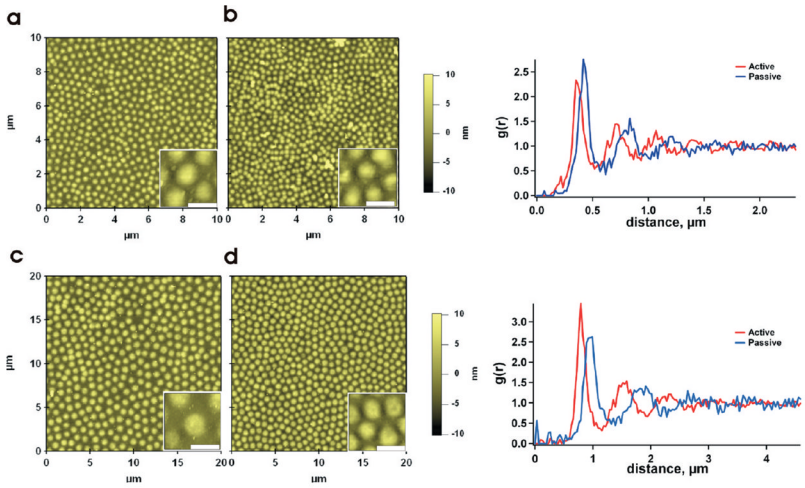

FIGURE 1.

Height traces, using AFM, of microgels 1 (a and b) and 2 (c and d) under passive deposition (a and c) and active centrifugal deposition (b and d). Microgels 1 and 2 were passively deposited for 16 h. Microgels 1 and 2 were actively deposited for 10 and 5 min, respectively. The inset scale bars are 0.5 μm (a and b) and 1 μm (c and d). On the right, radial distribution functions are shown for each particle type and deposition condition, illustrating the quantitative differences in the particle spacing between active and passive deposition.

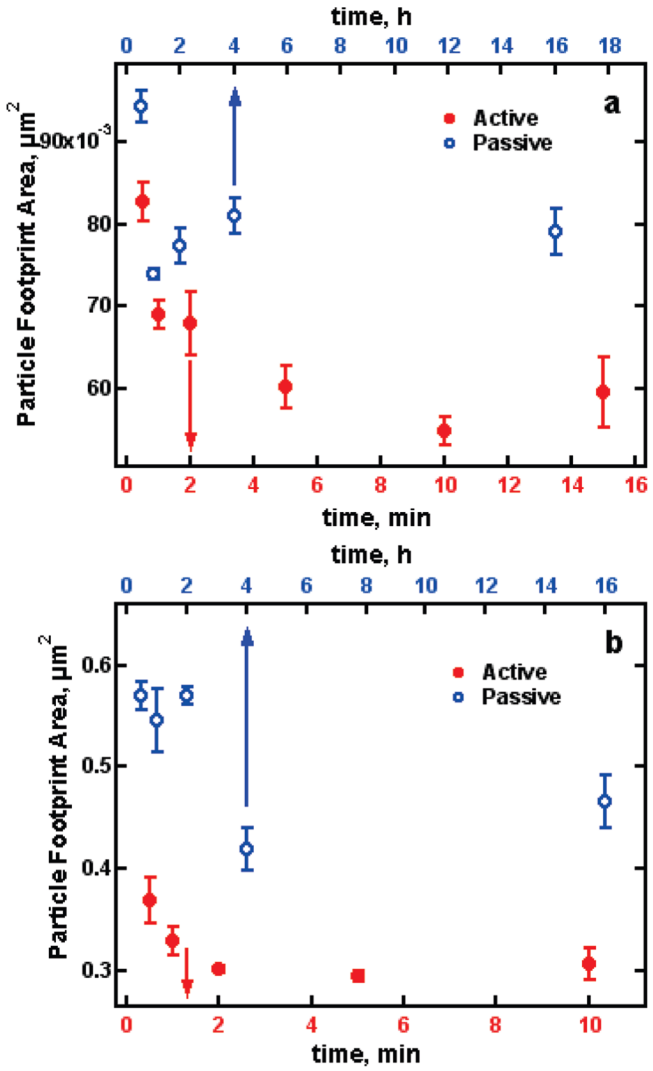

FIGURE 2.

Microgel footprint area as a function of the deposition time for centrifugation (active) and passive deposition techniques. Microgels: (a) 1 and (b) 2. Error bars represent the standard error of the mean particle footprint area taken from three 10 μm × 10 μm (a) or 20 μm × 20 μm (b) AFM images.

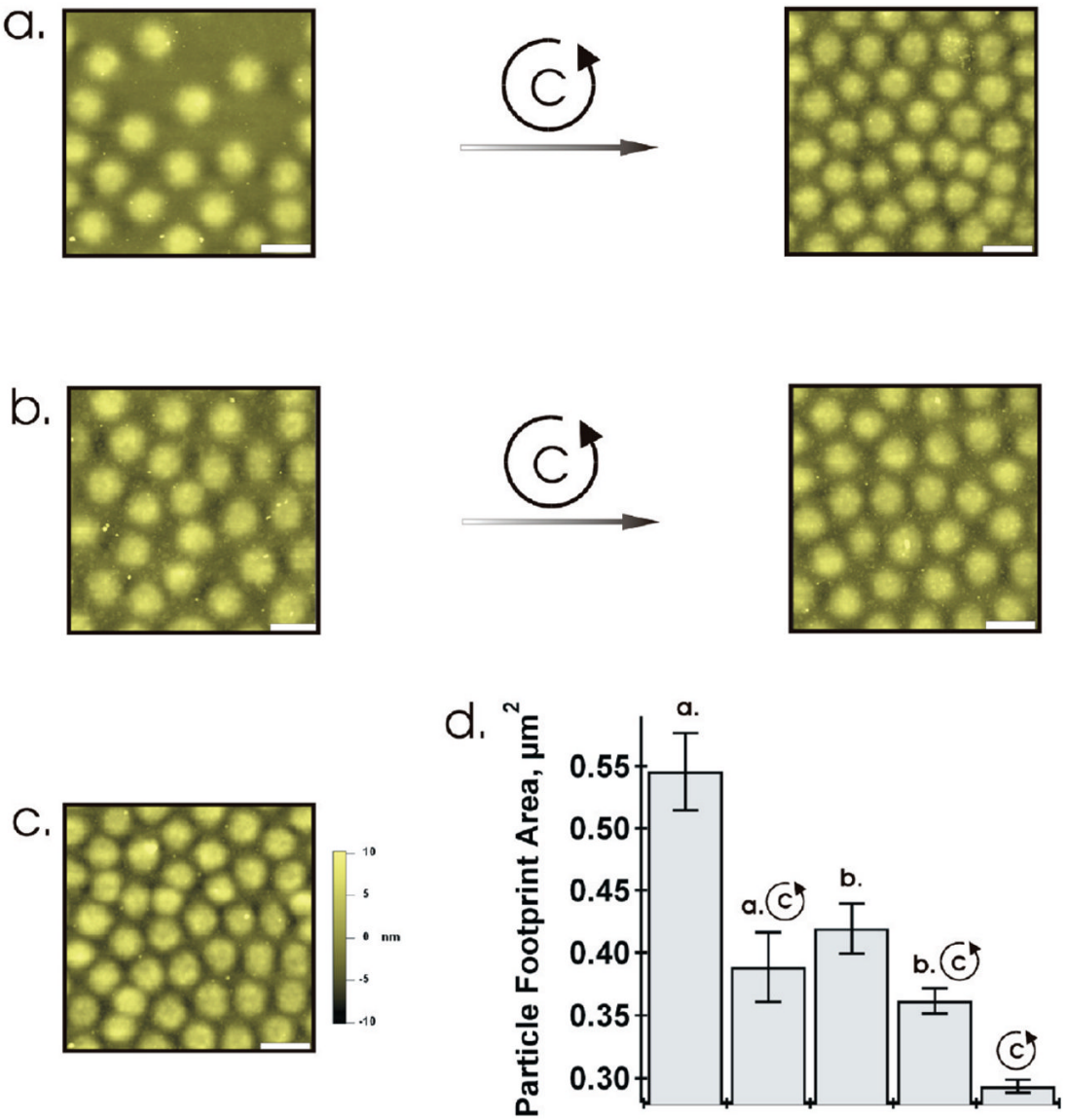

FIGURE 3.

Height traces, using AFM characterization, of the two-step deposition process for microgel 2. (a) A submonolayer, exhibiting patchy coverage, passively deposited first and then subjected to centrifugal deposition. (b) A higher coverage monolayer first deposited passively and then subjected to centrifugal deposition. (c) A high-coverage monolayer deposited under active conditions for comparison. Scale bar is 1 μm. (d) Bar graph showing the average particle footprint area for all samples. Error bars represent the standard error of the mean particle footprint area taken from three 20 μm × 20 μm AFM images.

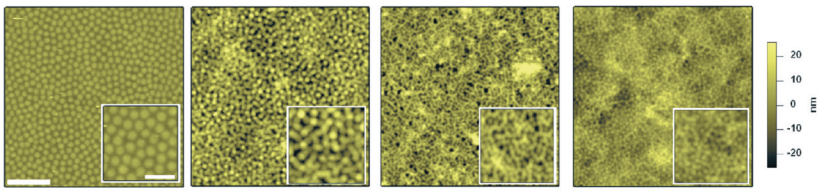

FIGURE 4.

AFM images of microgel thin films constructed in a multilayered fashion (using microgel 2). Each image has a 20 μm × 20 μm scan size (5 μm scale bar) with a 5 μm × 5 μm (2 μm scale bar) inset. Images were obtained from one-, two-, three-, and four-layer films (left to right) formed by active deposition.

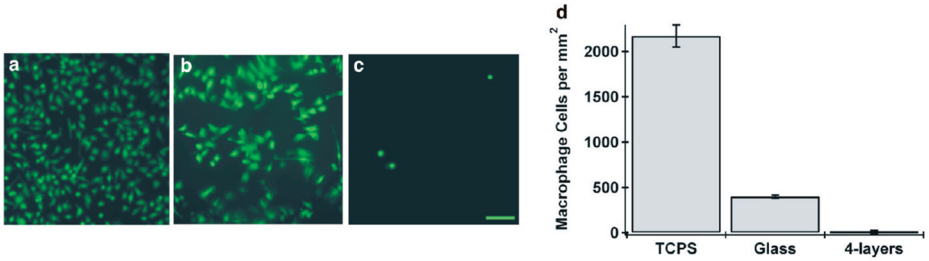

FIGURE 5.

Fluorescence microscopy of fluorescently stained macrophages adhering on (a) TCPS, (b) cleaned glass, and (c) four actively deposited layers of PEG-cross-linked pNIPAm microgels. The scale bar represents 100 μm. (d) Quantitative cellular adhesion from fluorescence microscopy images, with error bars representing the standard error.

Table 1

Microgel Properties

microgel	hydrodynamic radius, R_h (nm) at room temperature[a]	hydrodynamic radius, R_h (nm) at 40°C[a]	particle footprint area (nm^2)[b]	particle footprint area (nm^2)[c]	R_s/R_h	diffusion coefficient (cm^2/s)[a]	electrophoretic mobility ($m^2/s \cdot V$)[d]
1	171 ± 1 (15 ± 5% PD)	164 ± 1 (14 ± 2% PD)	$9.4 \times 10^4 \pm 2 \times 10^3$	$5.5 \times 10^4 \pm 2 \times 10^3$	1.01	$13.4 \pm 0.4 \times 10^{-9}$	-1.0×10^{-2}
2	365 ± 4 (14 ± 0.3% PD)	277 ± 4 (10 ± 2% PD)	$5.7 \times 10^5 \pm 1 \times 10^4$	$2.9 \times 10^5 \pm 2 \times 10^4$	1.17	$6.4 \pm 0.1 \times 10^{-9}$	-1.06×10^{-2}

[a] Determined by DLS in a pH 7.4 phosphate buffer containing 100 mM ionic strength (PBS) at room temperature.

[b] Determined by AFM on 30 min of passively deposited samples.

[c] Determined by AFM at the point of time of active deposition, where the particle footprint area was the smallest.

[d] Determined by electrophoretic light scattering in PBS at room temperature.

ACS Appl Mater Interfaces. Author manuscript; available in PMC 2010 August 2.